

# First-principles study of structural, vibrational, and lattice dielectric properties of hafnium oxide

Xinyuan Zhao and David Vanderbilt

Department of Physics and Astronomy, Rutgers University, Piscataway, New Jersey 08854-8019

(Received 25 February 2002; published 13 June 2002)

Crystalline structures, zone-center phonon modes, and the related dielectric response of the three low-pressure phases of  $\text{HfO}_2$  have been investigated in density-functional theory using ultrasoft pseudopotentials and a plane-wave basis. The structures of low-pressure  $\text{HfO}_2$  polymorphs are carefully studied with both the local-density approximation (LDA) and the generalized gradient approximation. The fully relaxed structures obtained with either exchange-correlation scheme agree reasonably well with experiment, although LDA yields better overall agreement. After calculating the Born effective charge tensors and the force-constant matrices by finite-difference methods, the lattice dielectric susceptibility tensors for the three  $\text{HfO}_2$  phases are computed by decomposing the tensors into the contributions from individual infrared-active phonon modes.

DOI: 10.1103/PhysRevB.65.233106

PACS number(s): 77.22.-d, 61.66.-f, 63.20.-e, 77.84.Bw

Hafnia ( $\text{HfO}_2$ ) is technologically important because of its extraordinary high bulk modulus, high melting point, and high chemical stability, as well as its high neutron absorption cross section.  $\text{HfO}_2$  resembles its twin oxide, zirconia ( $\text{ZrO}_2$ ), in many physical and chemical properties. The resemblance is attributable to the structural similarity between the two oxides, which can in turn be explained by the chemical similarity of Hf and Zr, which have similar atomic and ionic radii (i.e., ionic radii for  $\text{Hf}^{4+}$  and  $\text{Zr}^{4+}$  of 0.78 and 0.79 Å, respectively<sup>1</sup>) as a result of the so-called lanthanide contraction. Under ambient pressure, both oxides are monoclinic ( $m$ , space group  $P2_1/c$ ) at low temperature, and transform to a tetragonal structure ( $t$ , space group  $P4_2/nmc$ ) and then to a cubic structure ( $c$ , space group  $Fm\bar{3}m$ ) as the temperature increases, as illustrated in Fig. 1.

High-K metal-oxide dielectrics have recently been the focus of substantial ongoing efforts directed towards finding a replacement for  $\text{SiO}_2$  as the gate dielectric in complementary metal-oxide-semiconductor devices.  $\text{HfO}_2$ ,  $\text{ZrO}_2$ , and their  $\text{SiO}_2$  mixtures show promise for this purpose.<sup>2,3</sup> Thus, a systematic theoretical investigation of the structural and dielectric properties of these dielectrics, in both bulk and thin-film form, is clearly desirable. As a first step in this direction, we have, in a previous paper,<sup>4</sup> investigated the bulk structures and lattice dielectric response of  $\text{ZrO}_2$  polymorphs. We found that the dielectric responses vary dramatically with the crystal phase. Specifically, we found that the monoclinic phase has a strongly anisotropic lattice dielectric tensor and a rather small orientationally averaged dielectric constant owing to the fact that the mode effective charges associated with the softest modes are relatively weak.

This Brief Report presents the corresponding work on  $\text{HfO}_2$ , providing the first thorough theoretical study of the structural, vibrational, and lattice dielectric properties of the  $\text{HfO}_2$  phases. Such properties are naturally expected to be similar to those of  $\text{ZrO}_2$  in view of the chemical similarities mentioned above. We find that this is generally true, although we also find some significant quantitative differences in some of the calculated properties.

The calculation of the lattice contributions to the static dielectric tensor  $\epsilon_0$  entails the computations of the Born effective charge tensors  $\mathbf{Z}^*$  and the force-constant matrices  $\Phi$ .

The  $\mathbf{Z}^*$  tensors, defined via  $\Delta\mathbf{P}=(e/V)\sum_i\mathbf{Z}_i^*\cdot\Delta\mathbf{u}_i$ , are obtained by finite differences of polarizations ( $\mathbf{P}$ ) as various sublattice displacements ( $\mathbf{u}_i$ ) are imposed, with the electronic part of the polarizations computed using the Berry-phase approach.<sup>5,6</sup> Here  $V$  is the volume of the unit cell,  $e$  is the electron charge, and  $i$  labels the atom in the unit cell. We then calculate the force-constant matrix,  $\Phi_{ij}^{\alpha\beta}=-\partial F_i^\alpha/\partial u_j^\beta\approx-\Delta F_i^\alpha/\Delta u_j^\beta$  by calculating all the Hellmann-Feynman forces  $F_i^\alpha$  caused by making displacements  $u_j^\beta$  of each atom in each Cartesian direction in turn (Greek indices label the Cartesian coordinates). The resulting  $\Phi$  matrix is symmetrized to clean up numerical errors, the dynamical matrix  $D_{ij}^{\alpha\beta}=(M_iM_j)^{-1/2}\Phi_{ij}^{\alpha\beta}$  is constructed, and the latter is then diagonalized to obtain the eigenvalues  $\omega_\lambda^2$  and eigenvectors  $\xi_{i,\lambda\beta}$ .

The static dielectric tensor can be decomposed into a contribution  $\epsilon_\infty$  arising from purely electronic screening, and the contributions of the IR-active phonon modes, according to<sup>7</sup>

$$\epsilon_{\alpha\beta}^0=\epsilon_{\alpha\beta}^\infty+\frac{4\pi e^2}{M_0V}\sum_\lambda\frac{\tilde{Z}_{\lambda\alpha}^*\tilde{Z}_{\lambda\beta}^*}{\omega_\lambda^2}. \quad (1)$$

Here the  $\tilde{Z}_{\lambda\alpha}^*=\sum_{i\beta}\mathbf{Z}_{i,\alpha\beta}^*(M_0/M_i)^{1/2}\xi_{i,\lambda\beta}$  are mode effective charges,  $e$  is the electron charge,  $M_0$  is a reference mass that we take for convenience to be 1 amu,  $\omega_\lambda$  is the frequency of the  $\lambda$ th IR-active phonon mode, and  $V$  is the volume of the 3-atom, 6-atom, or 12-atom unit cell for cubic, tetragonal, or

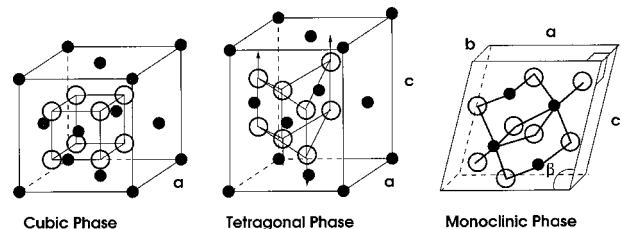


FIG. 1. Structures of the three  $\text{HfO}_2$  phases. Small dark circles and larger open circles denote Hf and O atoms respectively. Hf-O bonds are only shown in  $m$ - $\text{HfO}_2$ . In  $t$ - $\text{HfO}_2$ , the arrows indicate the shift of oxygen pairs.

TABLE I. Calculated structural parameters for three HfO<sub>2</sub> phases using both LDA and GGA. Lattice parameters  $a$ ,  $b$ ,  $c$  are in Å,  $\beta$  is in degrees, and  $V$  (volume per formula) is in Å<sup>3</sup>. Internal coordinates  $x$ ,  $y$  and  $z$  are dimensionless.

	Present LDA	Present GGA	Previous LDA <sup>a</sup>	Expt. <sup>b</sup>	ZrO <sub>2</sub> LDA <sup>c</sup>
Cubic					
$V$	31.95	36.15	32.01	32.77	31.95
$a$	5.037	5.248	5.04	5.08	5.037
Tetragonal					
$V$	32.77	37.74	32.5		32.26
$a$	5.056	5.299	5.03		5.029
$c$	5.127	5.373	5.11		5.100
$d_z$	0.042	0.041	0.038		0.041
Monoclinic					
$V$	34.35	38.01	33.9	34.58	34.35
$a$	5.106	5.291	5.08	5.117	5.108
$b$	5.165	5.405	5.19	5.175	5.170
$c$	5.281	5.366	5.22	5.291	5.272
$\beta$	99.35	97.92	99.77	99.22	99.21
$x_{\text{Hf}}$	0.280	0.276	0.280	0.276	0.277
$y_{\text{Hf}}$	0.043	0.039	0.044	0.040	0.042
$z_{\text{Hf}}$	0.209	0.209	0.208	0.208	0.210
$x_{\text{O}_1}$	0.076	0.089	0.078	0.074	0.069
$y_{\text{O}_1}$	0.346	0.367	0.350	0.332	0.333
$z_{\text{O}_1}$	0.337	0.317	0.332	0.347	0.345
$x_{\text{O}_2}$	0.447	0.447	0.446	0.449	0.450
$y_{\text{O}_2}$	0.759	0.762	0.759	0.758	0.757
$z_{\text{O}_2}$	0.483	0.488	0.485	0.480	0.480

<sup>a</sup>Reference. 13.

<sup>b</sup>Reference. 12 for cubic; Ref. 11 for monoclinic.

<sup>c</sup>Reference. 4.

monoclinic cases, respectively.  $\xi_{i,\lambda\beta}$ , the eigendisplacement of atom  $i$  in phonon mode  $\lambda$ , is normalized according to  $\sum_{i\alpha} \xi_{i,\lambda\alpha} \xi_{i,\lambda'\alpha} = \delta_{\lambda\lambda'}$ .

The calculations are carried out within an ultrasoft pseudopotential<sup>8</sup> implementation of density-functional theory with a plane-wave basis and a conjugate-gradient minimization algorithm. The crystal structures of HfO<sub>2</sub> polymorphs are investigated in the local-density approximation (LDA) as parametrized by Ceperley and Alder<sup>9</sup> as well as in the generalized gradient approximation (GGA) using Perdew-Burke-Ernzerhof (PBE) parametrization.<sup>10</sup> We find that LDA yields slightly better agreement with the experimental structures, and we therefore suggest that our LDA results for the dielectric properties are more reliable. The  $4s$  and  $4p$  semicore shells are included in the valence in the Hf pseudopotential, and an energy cutoff of 25 Ry is chosen. A  $4 \times 4 \times 4$  Monkhorst-Pack  $k$ -point mesh is found to provide sufficient precision in the calculations of total energies and forces, and a  $4 \times 4 \times 20$   $k$ -point sampling is used for calculating the Berry-phase polarization.<sup>5</sup> Each atomic sublattice is displaced in turn along each Cartesian direction by  $\pm 0.2\%$  in lattice units, the electronic polarization and Hellmann-

TABLE II. LDA dynamical effective charges  $\mathbf{Z}^*$  for HfO<sub>2</sub> phases. (Values in parentheses are GGA results.)

	Hf	O <sub>1</sub>	O <sub>2</sub>
Cubic			
	5.85	-2.93	-2.93
Tetragonal			
$x'x'$	5.84	-3.53	-2.31
$y'y'$	5.84	-2.31	-3.53
$zz$	5.00	-2.50	-2.50
Monoclinic			
$xx$	5.56 (5.57)	-3.09 (-3.10)	-2.48 (-2.47)
$xy$	-0.47 (-0.56)	0.97 (0.90)	0.20 (0.15)
$xz$	0.96 (0.91)	-0.58 (-0.53)	-0.39 (-0.36)
$yx$	-0.13 (-0.02)	1.37 (1.29)	0.21 (0.11)
$yy$	5.55 (5.57)	-2.73 (-2.70)	-2.82 (-2.87)
$yz$	0.14 (0.07)	-0.71 (-0.61)	0.35 (0.40)
$zx$	0.21 (0.27)	-0.18 (-0.20)	-0.07 (-0.09)
$zy$	0.41 (0.45)	-0.61 (-0.51)	0.43 (0.46)
$zz$	4.74 (4.64)	-2.24 (-2.16)	-2.58 (-2.52)

Feynman forces are computed, and  $\mathbf{Z}^*$  and  $\Phi$ , are then constructed by finite differences from the results.

Tabulated in Table I are the relaxed structural parameters for the three HfO<sub>2</sub> polymorphs, with the corresponding data for ZrO<sub>2</sub> listed in the last column for comparison.<sup>4</sup> While several structural determinations for  $m$ -HfO<sub>2</sub> can be found in the literature,<sup>1,11</sup> corresponding results for the tetragonal and cubic phases are relatively sparse.<sup>12</sup> Nor has there been much theoretical work on hafnia; most important is the recent work of Ref. 13 which agrees quite well with our results. For  $m$ -HfO<sub>2</sub>, the parameters given in Ref. 11 were used as the starting point of our relaxation procedures, while for  $t$ - and  $c$ -HfO<sub>2</sub> we started the relaxation from the zirconia experimental structures. It can readily be seen that both the LDA and GGA agree reasonably well with the previous work, but that the LDA yields a better overall agreement. Our total-energy calculations reproduce the correct energetic ordering of the phases (monoclinic then tetragonal then cubic) using either LDA or GGA.

Our results for the dynamical effective charges are presented in Table II. The symmetry of  $c$ -HfO<sub>2</sub> requires that  $\mathbf{Z}^*$  be isotropic on each atom. In  $t$ -HfO<sub>2</sub>, the shifting of oxygen atoms creates two different configurations for oxygen atoms (denoted O<sub>1</sub> and O<sub>2</sub>) and introduces off-diagonal elements. Thus, it is more natural to refer to a reference frame  $x'-y'-z$  that is rotated 45° about the  $\hat{z}$  axis from the original Cartesian frame.  $\mathbf{Z}^*(\text{O}_{1,2})$  become diagonal in this frame. In  $m$ -HfO<sub>2</sub>, there are two nonequivalent oxygen sites (i.e., the threefold and fourfold oxygens, labeled as O<sub>1</sub> and O<sub>2</sub> respectively). The crystal structure can then be regarded as composed of three kinds of atoms, namely, Zr, O<sub>1</sub>, and O<sub>2</sub>, which all have equally low symmetry, and their resulting  $\mathbf{Z}^*$  tensors are neither diagonal nor symmetric. The presence of two nonequivalent oxygen atoms with very different environments is reflected in the difference between the Born effec-

TABLE III. Theoretical (LDA and GGA) and experimental (Ref. 15) frequencies (in  $\text{cm}^{-1}$ ) of Raman-active phonon modes in monoclinic  $\text{HfO}_2$ .

Irrep	Mode	LDA	GGA	Expt. 15
$A_g$	1	128	125	113
	2	142	132	133
	3	152	171	149
	4	261	248	256
	5	326	339	323 <sup>a</sup>
	6	423	382	382
	7	514	440	498
	8	608	557	577
	9	738	640	672
$B_g$	1	131	120	133
	2	175	152	164
	3	250	223	242
	4	380	318	336
	5	424	385	398
	6	533	466	520
	7	570	529	551
	8	667	627	640
	9	821	716	773 <sup>b</sup>

<sup>a</sup>Unassigned.

<sup>b</sup>Reference. 17.

tive charge tensors for  $\text{O}_1$  and  $\text{O}_2$ . The anomalously large  $Z^*$  values indicate that there is a strong dynamic charge transfer along the Hf-O bond as the bond length varies, indicating a mixed ionic-covalent nature of the Hf-O bond. The resultant relatively delocalized distribution of the electronic charge is very similar to  $\text{ZrO}_2$ , and is quite common in partially covalent oxides.

Since  $\text{HfO}_2$  is isomorphic to  $\text{ZrO}_2$ , the analysis of the phonon modes at  $\Gamma$  is the same for  $\text{HfO}_2$  as for  $\text{ZrO}_2$ .<sup>4</sup> Of 36 phonon modes predicted for  $m$ - $\text{HfO}_2$ , 18 modes ( $9A_g + 9B_g$ ) are Raman active and 15 modes ( $8A_u + 7B_u$ ) are IR active, the remaining three modes being the zero-frequency translational modes. There are three IR-active modes ( $A_{2u}$  and two  $E_u$ ) and three Raman-active modes ( $A_{1g}$ ,  $B_{1g}$ , and  $E_g$ ) for  $t$ - $\text{HfO}_2$ . Only one IR-active mode (one  $T_{1u}$  triplet) is predicted for  $c$ - $\text{HfO}_2$ .

The Raman spectra of  $m$ - $\text{HfO}_2$  have been extensively measured experimentally,<sup>14–17</sup> but the situation is not entirely satisfactory.<sup>16</sup> Issues concerning the number of modes and the mode assignments still remain unresolved, partially because of sample impurities and the broadness and weakness of some observed features. Thus, our *ab-initio* theoretical calculation can play an important role in establishing the Raman assignments. Table III shows the frequencies of the  $A_g$  and  $B_g$  Raman-active modes as calculated in LDA and GGA, together with the observed frequencies from a polarized Raman measurement on a high-quality single crystal.<sup>15</sup> The agreement is generally excellent; the observed Raman shifts mostly fall comfortably in the LDA-GGA range. A later single-crystal (but unpolarized) Raman spectrum<sup>17</sup> shows almost identical mode frequencies. However, a few

TABLE IV. Frequencies  $\omega_\lambda$  ( $\text{cm}^{-1}$ ) and scalar mode effective charges  $\tilde{Z}_\lambda^*$  of IR-active phonon modes for  $\text{HfO}_2$  phases, where  $\tilde{Z}_\lambda^{*2} = \sum_\alpha \tilde{Z}_{\lambda\alpha}^{*2}$ .

Irrep	LDA		GGA	
	$\omega_\lambda$	$\tilde{Z}_\lambda^*$	$\omega_\lambda$	$\tilde{Z}_\lambda^*$
Cubic				
1	$T_{1u}$	286	1.12	
Tetragonal				
1	$E_u$	117	1.26	
2	$A_{2u}$	384	1.45	
3	$E_u$	536	1.13	
Monoclinic				
1	$A_u$	140	0.049	123
2	$A_u$	190	0.003	162
3	$B_u$	246	0.887	223
4	$A_u$	255	0.764	250
5	$B_u$	262	0.121	252
6	$B_u$	354	1.623	300
7	$B_u$	378	1.126	331
8	$A_u$	393	1.148	360
9	$A_u$	445	1.218	391
10	$B_u$	449	1.497	414
11	$A_u$	529	0.836	456
12	$B_u$	553	0.810	494
13	$A_u$	661	0.788	577
14	$A_u$	683	0.688	634
15	$B_u$	779	0.997	694

details about the Table deserve comment. (i) We omit the weak mode reported as  $A_g$  at  $268 \text{ cm}^{-1}$  in Ref. 15 because it is not confirmed in Ref. 17 and it does not fit with our theoretical assignments. (ii) We assign the  $323 \text{ cm}^{-1}$  mode observed in Refs. 15 and 17 as  $A_g$ . (iii) The feature observed at  $872 \text{ cm}^{-1}$  in Ref. 15 is presumed to be a two-phonon process and is omitted. (iv) A weak mode is observed at  $773 \text{ cm}^{-1}$  in Ref. 17; since this is consistent with our highest-frequency  $B_g$  mode, we assign it as such.

The frequencies of the IR-active phonon modes for the three  $\text{HfO}_2$  phases are tabulated in Table IV together with the scalar mode effective charges. It can be seen that the frequencies calculated in GGA are shifted to lower frequency by  $\sim 10$ – $16\%$  relative to the LDA ones, while the mode assignments coincide exactly. As indicated in Eq. (1), the contribution of a given IR-active mode to the static dielectric constant scales as  $\tilde{Z}^{*2}/\omega_\lambda^2$ ,<sup>4</sup> so that one or more low-frequency modes with large  $\tilde{Z}^*$ 's are needed to yield a large dielectric constant. As can be seen from Table IV however, the few softest modes ( $< 300 \text{ cm}^{-1}$ ) have relatively small  $\tilde{Z}^*$ 's, while the more active infrared modes come in the intermediate range of the IR spectrum ( $350$ – $450 \text{ cm}^{-1}$ ). The general pattern is very similar to the case of  $\text{ZrO}_2$ .

The lattice contributions to the dielectric tensors are obtained by summing the second term of Eq. (1) over all the IR-active modes. Using the LDA we find

$$\epsilon_{\text{cubic}}^{\text{latt}} = \begin{pmatrix} 23.9 & 0 & 0 \\ 0 & 23.9 & 0 \\ 0 & 0 & 23.9 \end{pmatrix},$$

$$\epsilon_{\text{tetra}}^{\text{latt}} = \begin{pmatrix} 92.3 & 0 & 0 \\ 0 & 92.3 & 0 \\ 0 & 0 & 10.7 \end{pmatrix},$$

$$\epsilon_{\text{mono}}^{\text{latt}} = \begin{pmatrix} 13.1 & 0 & 1.82 \\ 0 & 10.8 & 0 \\ 1.82 & 0 & 7.53 \end{pmatrix}.$$

(The corresponding matrix elements of  $\epsilon_{\text{mono}}^{\text{latt}}$  in the GGA tend to be larger than the LDA results by  $\sim 18\%$ .) When compared with  $\text{ZrO}_2$ , the off-diagonal elements of  $\epsilon_{\text{mono}}^{\text{latt}}$  are roughly doubled, while the diagonal elements become smaller. Most surprisingly, the  $x$ - $y$  components of  $\epsilon_{\text{tetra}}^{\text{latt}}$  become more than twice as large as for  $\text{ZrO}_2$ , while the  $z$  component decreases by  $\sim 28\%$ . We find the isotropic  $\epsilon_{\text{cubic}}^{\text{latt}}$  to be 23.9, somewhat smaller than the value of 31.8 for  $\text{ZrO}_2$ .<sup>4</sup>

A direct comparison of these dielectric tensors with experiment is not feasible since there are few experimental measurements, especially on the cubic and tetragonal phases. On the other hand, most measurements of which we are

aware have been carried out on thin films (presumed to be monoclinic), and the reported dielectric constants span a wide range of 16–45.<sup>3,18,19</sup> Assuming an isotropic  $\epsilon_{\infty} \approx 5$ ,<sup>4</sup> we obtained orientationally averaged static dielectric constants of 29, 70, and 16 (18 in GGA) for the cubic, tetragonal, and monoclinic  $\text{HfO}_2$  phases, respectively. Our results then agree reasonably well with the more recent results in Ref. 19 (thin film  $\sim 1700$  Å) and Ref. 3 (ultrathin film  $< 100$  Å) which report  $\epsilon_0$  to be 16 and 20 respectively. The surprisingly high  $\epsilon_0$  measured in other experiments could possibly be explained by the presence of  $t$ - $\text{HfO}_2$ , which is known to be a metastable phase and which might be stabilized by film stress or grain-size effects.<sup>12,19,20</sup>

In summary, we have investigated here the Born effective charge tensors, zone-centered phonons, and the lattice contributions to the static dielectric tensors for the three  $\text{HfO}_2$  phases. It is found that the cubic and tetragonal phases have much larger dielectric response than the monoclinic phase, with an even stronger anisotropy in  $t$ - $\text{HfO}_2$  than in  $t$ - $\text{ZrO}_2$ . The overall dielectric constants for  $c$ - $\text{HfO}_2$  and  $m$ - $\text{HfO}_2$  are found to become smaller, while  $t$ - $\text{HfO}_2$  has a much greater dielectric constant, than the corresponding values in  $\text{ZrO}_2$ . Moreover, our Raman results can be used in resolving the puzzles associated with the Raman spectrum for  $m$ - $\text{HfO}_2$ .

This work has been supported by NSF Grant No. DMR-99-81193. We wish to thank E. Garfunkel for useful discussions.

- 
- <sup>1</sup>R. Ruh and P.W.R. Corfield, *J. Am. Ceram. Soc.* **53**, 126 (1970).  
<sup>2</sup>G.D. Wilk, R.M. Wallace, and J.M. Anthony, *J. Appl. Phys.* **89**, 5243 (2001).  
<sup>3</sup>E.P. Gusev, E. Cartier, D.A. Buchanan, M. Gribelyuk, M. Copel, H. Okorn-Schmidt, and C. D'Emic, *Microelectron. Eng.* **59**, 341 (2001).  
<sup>4</sup>X. Zhao and D. Vanderbilt, *Phys. Rev. B* **65**, 075105 (2002).  
<sup>5</sup>R.D. King-Smith and D. Vanderbilt, *Phys. Rev. B* **47**, 1651 (1993).  
<sup>6</sup>R. Resta, M. Posternak, and A. Baldereschi, *Phys. Rev. Lett.* **70**, 1010 (1993).  
<sup>7</sup>All three  $\text{HfO}_2$  phases are non-piezoelectric, so the fixed-strain and free-stress dielectric tensors are identical for these systems.  
<sup>8</sup>D. Vanderbilt, *Phys. Rev. B* **41**, 7892 (1990).  
<sup>9</sup>D.M. Ceperley and B.J. Alder, *Phys. Rev. Lett.* **45**, 566 (1980).  
<sup>10</sup>J.P. Perdew, K. Burke, and M. Ernzerhof, *Phys. Rev. Lett.* **77**, 3865 (1996); Y. Zhang and W. Yang, *ibid.* **80**, 890 (1998).  
<sup>11</sup>J. Adam and M.D. Rodgers, *Acta Crystallogr.* **12**, 951 (1959);  
R.E. Hann, P.R. Suttch, and J.L. Pentecost, *J. Am. Ceram. Soc.* **68**, C-285 (1985).  
<sup>12</sup>J. Wang, H.P. Li, and R. Stivens, *J. Mater. Sci.* **27**, 5397 (1992).  
<sup>13</sup>A.A. Demkov, *Phys. Status Solidi B* **226**, 57 (2001).  
<sup>14</sup>E. Anastassakis, B. Papanicolaou, and I.M. Asher, *J. Phys. Chem. Solids* **36**, 667 (1975).  
<sup>15</sup>H. Arashi, *J. Am. Ceram. Soc.* **75**, 844 (1992).  
<sup>16</sup>C. Carlone, *Phys. Rev. B* **45**, 2079 (1992).  
<sup>17</sup>A. Jayaraman, S.Y. Wang, S.K. Sharma, and L.C. Ming, *Phys. Rev. B* **48**, 9205 (1993).  
<sup>18</sup>P.J. Harrop and D.S. Campell, *Thin Solid Films* **2**, 273 (1968); M. Balog, M. Schieber, M. Michman, and S. Patai, *J. Elec. Chem. Soc.* **126**, 1203 (1979); C.T. Hsu, Y.K. Su, and M. Yokoyama, *Jpn. J. Appl. Phys.* **31**, 2501 (1992).  
<sup>19</sup>K. Kukli, J. Ihanus, M. Ritala, and M. Leskela, *Appl. Phys. Lett.* **68**, 3737 (1996).  
<sup>20</sup>R.C. Garvie, *J. Phys. Chem.* **82**, 218 (1978).